

Uniting the Quiescent Emission and Burst Spectra of Magnetar Candidates

Yujin E. Nakagawa,^{1,2} Atsumasa Yoshida,¹ Kazutaka Yamaoka,¹ Noriaki Shibazaki,³

¹Graduate School of Science and Engineering, Aoyama Gakuin University, 5-10-1 Fuchinobe, Sagami-hara, Kanagawa 229-8558

yujin@crab.riken.jp

²Institute of Physical and Chemical Research (RIKEN), 2-1 Hirosawa, Wako, Saitama 351-0198

³Department of Physics, Rikkyo University, Nishi-Ikebukuro, Toshima-ku, Tokyo 171-8501

(Received 2007 October 20; accepted 2008 October 7)

Abstract

Spectral studies of quiescent emission and bursts of magnetar candidates using XMM-Newton, *Chandra* and *Swift* data are presented. Spectra of both the quiescent emission and the bursts for most magnetar candidates are reproduced by a photoelectrically absorbed two blackbody function (2BB). There is a strong correlation between lower and higher temperatures of 2BB (kT_{LT} and kT_{HT}) for the magnetar candidates of which the spectra are well reproduced by 2BB. In addition, a square of radius for kT_{LT} (R_{LT}^2) is well correlated with a square of radius for kT_{HT} (R_{HT}^2). A ratio $kT_{LT}/kT_{HT} \approx 0.4$ is nearly constant irrespective of objects and/or emission types (i.e., the quiescent emission and the bursts). This would imply a common emission mechanism among the magnetar candidates. The relation between the quiescent emission and the bursts might be analogous to a relation between microflares and solar flares of the sun. Three AXPs (4U 0142+614, 1RXS J170849.0–400910 and 1E 2259+586) seem to have an excess above ~ 7 keV which well agrees with a non-thermal hard component discovered by INTEGRAL.

Key words: stars pulsars: general – X-rays: stars

1. Introduction

Among peculiar celestial objects in the universe, a dense highly magnetized neutron star ($\rho \sim 10^{14}$ g cm⁻³ and $B \sim 10^{15}$ G), so-called “magnetar” (Duncan & Thompson 1992; Paczyński 1992; Thompson & Duncan 1995; Thompson & Duncan 1996), would be one of the most exotic objects. Soft gamma repeaters (SGRs) and anomalous X-ray pulsars (AXPs) are well known as magnetar candidates. An apparent difference between the SGRs and the AXPs would be considered from their first detections. The SGRs were discovered as sporadically bursting objects, while the AXPs were regarded as peculiar pulsars with long spin periods. However, current observations unveil a lot of similarities between these objects. They have, for instance, long spin periods ($P \sim 5$ –12 s) with spindown rates of $\dot{P} \sim 10^{-10}$ – 10^{-13} s s⁻¹, no signature of a companion star, a distribution around the galactic plane (two magnetar candidates are in other galaxies), quiescent soft X-ray emission. Several of these objects have non-thermal hard (> 20 keV) components, some are associated with supernova remnants (SNRs), and bursting activity is not confined to the SGRs but is observed in the AXPs as well. Considering these similarities, the SGRs and the AXPs should be classified into a common class of objects.

So far, five SGRs (0501+4516, 0526–66, 1627–41, 1806–20 and 1900+14) are known (Woods & Thompson 2006; Barthelmy et al. 2008) as well as three candidates, SGR 1801–23 (Cline et al. 2000),

SGR 1808–20 (Lamb et al. 2003) and SGR/GRB 050925. SGR/GRB 050925 was regarded as a gamma-ray burst (GRB) when first detected, but soon after was recognized as a new SGR (Holland et al. 2005). On the other hand, ten AXPs (1E 2259+586, 1E 1048.1–5937, 4U 0142+614, 1RXS J170849.0–400910, 1E 1841–045, XTE J1810–197, AX J1845–0258, CXOU J010043.1–721134, CXOU J164710.2–455216 and 1E 1547.0–5408) are known to date (Woods & Thompson 2006; Dib et al. 2008) with one AXP candidate, AXP CXOU J160103.1–513353 (Park et al. 2006). A short burst from AXP CXOU J164710.2–455216 was detected by *Swift* BAT (Krimm et al. 2006) at 01:34:52 on 2006 September 21. The follow-up observations performed by *Swift* XRT found a remarkable result in which the quiescent emission of post-burst became 190 times brighter than that of pre-burst (Campana & Israel 2006). In addition to these objects, AX J1818.8–1559 discovered by ASCA (Sugizaki et al. 2001) recently exhibited a short burst (Mereghetti et al. 2007) similar to those from the magnetar candidates. Therefore AX J1818.8–1559 could be a new SGR or AXP (Mereghetti et al. 2007).

The most exciting phenomena among the magnetar candidates would be a sudden release of huge energy in rather short period, the so-called *giant flares* from the SGRs. They typically have a short intense spike which last less than 1 s, and followed by a long pulsating tail which lasts a few hundred seconds. Their peak energy flux can be larger than $\sim 10^6$ times Eddington luminosity. Theoretical studies suggested that the giant flares were triggered by

a catastrophic deformation of the neutron star crust due to a torsion of the strong magnetic field (e.g., Thompson & Duncan 2001). Some different emission mechanisms have been proposed by several authors (Yamazaki et al. 2005; Lyutikov 2006; Cea 2006). In the past three decades, three giant flares were recorded. The first detection, from the source now known as SGR 0526–66 in Large Magellanic Cloud (LMC), was made on March 5 in 1979 (Mazets, Golenetskii & Gur’yan 1979; Cline et al. 1980; Evans et al. 1980; Fenimore, Klebesadel & Laros 1996). The second one from SGR 1900+14 was recorded on August 27 in 1998 (Hurley et al. 1999b; Feroci et al. 1999; Mazets et al. 1999; Feroci et al. 2001; Tanaka et al. 2007). More recently, the most energetic giant flare from SGR 1806–20 was observed on December 27 in 2004 (Cameron et al. 2005; Gaensler et al. 2005; Hurley et al. 2005; Mazets et al. 2005; Palmer et al. 2005; Terasawa et al. 2005; Tanaka et al. 2007). The fluence of its initial intense spike with 600 ms was evaluated to be $\sim 2 \text{ erg cm}^{-2}$ by the plasma particle detectors on the Geotail space probe (Terasawa et al. 2005).

Soft X-ray spectra of the quiescent emission of the SGRs and the AXPs were observed by a number of satellites. Although their spectral model is still under discussion, two two-component models are proposed. One of them is a photoelectrically absorbed two blackbody function (2BB). Spectral parameters of 2BB are reported by some authors for the SGRs (Mereghetti et al. 2006a) and the AXPs (Tiengo et al. 2002; Morii et al. 2003; Gotthelf et al. 2004; Gotthelf & Halpern 2005; Halpern & Gotthelf 2005; Tiengo et al. 2005; Israel et al. 2006; Gotthelf & Halpern 2007). Typical lower and higher temperatures are $\sim 0.5 \text{ keV}$ and $\sim 1.4 \text{ keV}$, respectively. The other model is a photoelectrically absorbed power law plus a blackbody (PL+BB). Some authors report spectral parameters of PL+BB for the SGRs (Marsden & White 2001; Kurkarni et al. 2003; Mereghetti et al. 2005; Mereghetti et al. 2006a; Mereghetti, Esposito & Tiengo 2007) and the AXPs (Morii et al. 2003; Patel et al. 2003; Rea et al. 2003; Gotthelf et al. 2004; Mereghetti et al. 2004; Woods et al. 2004; Tiengo et al. 2005; Gavriil, Kaspi & Woods 2006; Israel et al. 2006). A typical power law index and a blackbody temperature are ~ 3 and $\sim 0.5 \text{ keV}$. At present it is still unclear which model is more reliable or physically suitable.

Recent observations by the International Gamma-Ray Astrophysics Laboratory (INTEGRAL) discovered a non-thermal hard component in the spectra of the quiescent emission above 20 keV for 5 magnetar candidates (Molkov et al. 2005; Götz et al. 2006b; Kuiper et al. 2006). The non-thermal hard component is well reproduced by a power law model, $E^{-\Gamma}$, where Γ ranges from 1.0–1.8, while the soft X-ray emission below $\sim 12 \text{ keV}$, mentioned above, clearly indicates steeper power-law index of ~ 3 if the PL+BB is applied as the model spectrum. Hence, the non-thermal hard emission seen by INTEGRAL is a different component and presumably has a different origin than the soft X-ray emission. Since some magnetar candidates have two different emission mechanisms, there seems to be

more complex physics than expected before. Moreover, the non-thermal hard component shows pulsations for three AXPs, 1RXS J170849.0–400910, 4U 0142+614 and 1E 1841–045, through the INTEGRAL and RXTE observations (Kuiper et al. 2006), which is related to a neutron star rotation, and hence there are particle acceleration processes in the vicinity of neutron stars (Kuiper et al. 2006).

If the energy source of the quiescent emission and the bursts is the magnetic field as thought to be, at least very similar physical process would govern both of them and their spectra could emerge alike. It is claimed based on High Energy Transient Explorer 2 (HETE-2) data that the most acceptable spectral model of the short bursts from two SGRs 180620 and 1900+14 is 2BB even though it should be regarded just as an empirical model (Nakagawa et al. 2007). It would be also preferred to represent spectra of quiescent emissions by 2BB rather than BB+PL for SGRs, and even for AXPs if it is the same class of object. In this paper, we present a comprehensive spectral study with 2BB for both the quiescent emission and the for the magnetar candidates.

2. Data Analyses of Magnetar Candidates

2.1. Samples of Magnetar Candidates for Spectral Analyses

Among magnetar candidates, three SGRs (0526–66, 1627–41 and 1806–20), one SGR candidate (GRB/SGR 050925), six AXPs (CXOU J010043.1–721134, 4U 0142+614, CXOU J164710.2–455216, 1RXS J170849.0–400910, 1E 1841–045 and 1E 2259+586) and a possible SGR or AXP candidate AX J1818.8–1559 were used in our study. For the sake of convenience, we shall refer to GRB/SGR 050925 and AX J1818.8–1559 according to the naming convention for SGRs, i.e., SGR 2013+34 and SGR 1819–16. Since results of spectral analyses with a photoelectrically absorbed two blackbody function (2BB) using data derived from XMM-Newton observations are reported for SGR 1900+14 (Mereghetti et al. 2006a), AXP 1E 1048.1–5937 (Tiengo et al. 2005) and AXP XTE J1810–197 (Gotthelf et al. 2004; Gotthelf & Halpern 2005), these data were not analyzed in our study. Two SGR candidates (1801–23 and 1808–20) were not also included in the analysis nor the X-ray counterpart of AXP AX J1845–0258 (Tam et al. 2006) since its location is still uncertain. An AXP candidate CXOU J160103.1–513353 was also not utilized, because *Chandra* observations are not archived at this point. Table 1 shows a summary of utilized magnetar candidates in our study. In this paper, we analyzed both the quiescent emission and the short bursts of the magnetar candidates.

Observations of the quiescent emission utilized in our study were from the European Photon Imaging Camera (EPIC; Turner et al. 2001; Strüder et al. 2001) on-board XMM-Newton (Jansen et al. 2001), the Advanced CCD Imaging Spectrometer (ACIS) on-board *Chandra* and the

X-ray Telescope (XRT; Burrows et al. 2005) on-board *Swift* (Gehrels et al. 2004). The short bursts were observed by the Burst Alert Telescope (BAT, Barthelmy et al. 2005). Among the three observational modes (pointing, slew and settling phase) of *Swift* XRT (Capaldi et al. 2005)¹, only data in pointing mode were utilized. The data observed by XMM-Newton and *Chandra* with a timing mode, and by *Chandra* with a grating mode were not used to reduce spectral uncertainties.

2.2. Distances to Magnetar Candidates

Despite careful measurements by many satellites and ground telescopes, distances to the SGRs and the AXPs are still very uncertain. In this paper, we used the distances in table 1 (see Woods & Thompson 2006 and references therein). Park et al. (2006) suggested $d \sim 5$ kpc for AXP CXOU J160103.1–513353, if this source is associated with a SNR G330.2+1.0. If AXP CXOU J164710.2–455216 is related to the cluster Westerlund 1, the distance might be $d \sim 5$ kpc (Muno et al. 2006). Since there are no measurements of the distances to two SGRs 2013+34 and 1819–16, their distances are assumed to be $d = 10$ kpc. The blackbody radii in this paper were calculated using the distances in table 1.

2.3. Data Reductions

2.3.1. XMM-Newton

The data reductions for XMM-Newton observations were made using the SAS 7.0.0 software in the following way. To apply the latest calibration results to the data, the basic pipeline processing using the SAS tasks *emchain* and *epchain* were performed. Proton flares are usually seen in the light curves of these observations (Snowden et al. 2004)². If the count rate of the proton flare is large compared with the nominal background, the proton flare cannot be ignored in the spectral analyses. Therefore those high background time regions were excluded using a threshold of twice the nominal background. The effects of photon pile-up were investigated using *epatplot* for each observation. The circular foreground and background regions were determined by eye and their spectra were extracted using *xmmselect*. The response matrix files and the auxiliary response files were calculated using *rmfgen* and *arfgen*. We only considered phptons in the 0.6–12 keV band.

2.3.2. Chandra

The data reductions for *Chandra* observations were made using the CIAO 3.3 software in the following way. Since some observations were not applied to the latest calibration results, the new Level=2 event files were created for these observations. First, the *acis_detect_afterglow* corrections were removed using the CIAO tool *dmtcalc*. After that, hot pixels and cosmic ray afterglows were identified using *acis_run_hotpix*. Then, the new Level=2 event files were created using *acis_process_events*. Using the data

applied to the latest calibration results, the circular foreground and background regions were determined by eye, and their spectra were extracted using *dmextract*. The response matrix files were calculated using *acis_fef_lookup* and *mkrmf*. The auxiliary response files were calculated using *asphist* and *mkarf*. We only considered phptons in the 0.1–6 keV band.

2.3.3. Swift BAT

The data reductions for *Swift* observations were made using the HEASoft 6.1.1 software. For the data reductions of *Swift* BAT, the following steps were performed. Light curves in 15–150 keV were generated using *batbinevt*, and the foreground time regions were determined by eye for each burst. The foreground spectra were generated with those time regions using *batbinevt*. The background was already subtracted using a mask weighting method by the *Swift* Data Center. Corrections due to the spacecraft slewing during a burst were applied to the foreground spectral files using *batupdatephakw*. The systematic errors recommended by the BAT team were applied to the foreground spectral files using *batphasyserr*. The response matrix files were calculated using *batdrngen*. We only used photons in the 15–15 keV band.

2.3.4. Swift XRT

To reduce the *Swift* XRT data we performed the following. We generated the Level 2 (screened) event files using the pipeline processing tool *xrtpipeline*. The effects of photon pile-up were investigated following the methods described by Romano et al. (2006). The foreground and background regions were determined with a rectangle for WT mode and a circle for PC mode selected by eye. The spectra were extracted using XSELECT V2.3 which is part of the HEASoft 6.1.1 software package. The auxiliary response files were calculated using *xrtmkarf*. The response matrix files included in CALDB 20060407 were utilized. We only considered photons in the 0.6–10 keV band.

2.4. Observations and Spectral Analyses

A recent study using HETE-2 data by Nakagawa et al. (2007) revealed that the most acceptable spectral model for the SGR short bursts is a 2BB. If the bursts and the quiescent emission are both activated by magnetic dissipation, the quiescent emission spectra may be reproduced by the same spectral model for the bursts (i.e., 2BB). Then we performed the spectral analyses with a 2BB model for both the short bursts and the quiescent emission for all samples. If reliable temperatures and/or radii were not determined using 2BB because of insufficient statistics due to small exposure times and/or a faint object, a photoelectrically absorbed single blackbody (BB) was used. Note that because the spectral analyses of the short bursts detected by *Swift* BAT were performed using data above 15 keV, a photoelectric absorption was not required.

Photon pile-up effect was negligible for all observations utilized here. We used shapes and sizes of the foreground and background regions presented in subsection 2.3 and tables 2–6, respectively. The spectral fits were performed with XSPEC 12.3.0 (Arnaud 1996) in HEASoft 6.1.1 soft-

¹ This document is available at http://heasarc.gsfc.nasa.gov/docs/swift/analysis/xrt_swguide_v1.2.pdf.

² This document is available at ftp://legacy.gsfc.nasa.gov/xmm/doc/xmm_abc_guide.pdf

ware. The spectra were binned to at least 25 counts in each spectral bin using *grpppha*. The spectral parameters are summarized in table 7-12, where the quoted errors are 68 % confidence level for fluxes and 90 % confidence level for other parameters.

2.4.1. SGR 0526–66

SGR 0526–66 was observed at three epochs by *Chandra* from 2000 to 2001. Two observations were utilized in our study (table 3), because one observation on 2001 September 1 was affected by a photon pile-up effect (Kurkarni et al. 2003). The spectra were well reproduced by 2BB (table 8).

Two XMM-Newton observations from 2000 to 2001 were not utilized, because we could not distinguish between SGR 0526–66 and its SNR.

2.4.2. SGR 1627–41

SGR 1627–41 was observed at three epochs by XMM-Newton in 2004 (table 2). Since the spectral fits with 2BB could not give reliable lower and higher temperatures (kT_{LT} and kT_{HT}), BB was used (table 7).

This object was also observed at 4 epochs by *Chandra* from 2001 to 2005. Two observations were utilized (table 3), because one observation on 2003 April 21 was performed with a timing mode and one observation on 2005 June 28 had less statistics due to small net exposure time (9.83 ks). The spectra were reproduced by BB (table 8), because reliable kT_{LT} and kT_{HT} could not be obtained by 2BB.

2.4.3. SGR 1806–20

SGR 1806–20 was observed at 6 epochs by XMM-Newton from 2003 to 2005 (table 2). Among them, 4 observations were performed before the giant flare on 2004 December 27, while the other two observations were performed after it. The spectra were well reproduced by 2BB (table 7).

This object was also observed at 11 epochs by *Chandra* from 2000 to 2006. The *Chandra* observations were not utilized in our study, because three imaging observations were affected by a photon pile-up effect (Kaplan et al. 2002).

2.4.4. Burst on 2005 September 25 - A Candidate of SGR

We analyzed the short burst from SGR 2013+34 (Holland et al. 2005). The burst spectrum was generated using the *Swift* BAT data from 0.06 s to 0.17 s and well reproduced by 2BB (table 9).

The X-ray counterpart was observed at 4 epochs by *Swift* XRT from 2005 to 2006. These observations were not utilized in our study, because we could not find the X-ray counterpart or there was practically no exposure time for the WT mode. For PC mode, there was not enough statistics to perform the spectral analyses.

The follow-up observation by XMM-Newton (table 2) also detected the X-ray counterpart (De Luca et al. 2005). The spectrum was reproduced by BB (table 7), because reliable spectral parameters were not obtained by 2BB.

2.5. Burst on 2007 October 17 - A Candidate of SGR or AXP

We analyzed the short burst from SGR 1819–16 (Mereghetti et al. 2007). This object was observed at one epoch by XMM-Newton in 2003 (table 2). Since reliable spectral parameters were not obtained by 2BB, BB was used (table 7). In table 7, the temperature is a little bit larger than a typical value for the SGRs and AXPs (see figure 3) as already reported by Tiengo et al. (2007). Note that a photoelectrically absorbed power law model (PL) also gave an acceptable result of $\chi^2/\text{d.o.f.} = 56/74$, which is consistent with a result reported by Tiengo et al. (2007). Further observations should be encouraged to reveal whether SGR 1819–16 is a new SGR or AXP.

2.5.1. AXP CXOU J010043.1–721134

AXP CXOU J010043.1–721134 was observed at three epochs by XMM-Newton from 2000 to 2005. One observation on 2005 March 27 was not utilized in our study, because the pn camera was not operated, and the object fell on a gap of the CCD chips for the MOS1 and MOS2 cameras. For the other two observations (table 4), the data of the pn and MOS1 cameras were utilized in our study, because the object fell on a gap of the CCD chips for the MOS2 camera. The spectra were well reproduced by 2BB (table 10).

AXP CXOU J010043.1–721134 was also observed at 6 epochs by *Chandra* from 2001 to 2004 (table 4). The spectra for three observations were well reproduced by 2BB, while the spectra of the other three observations were reproduced by BB because reliable kT_{LT} could not be obtained by 2BB (see table 11).

2.5.2. AXP 4U 0142+614

AXP 4U 0142+614 was observed at 4 epochs by XMM-Newton from 2002 to 2004. One observation on 2002 February 13 was not utilized in our study, because the background level became 10 times higher than the ordinary background level (Göhler, Wilms & Staubert 2005). We just utilized one observation on 2003 January 24 by the pn camera (table 4), because the other observations were performed with a timing mode or affected by pile-up. The spectrum was not reproduced by a 2BB ($\chi^2/\text{d.o.f.} = 1086/819$), because there seems to be an excess above ~ 7 keV (table 10).

This object was also observed at 4 epochs by *Chandra* from 2000 to 2006. Although three observations were archived, we did not utilize them because they were affected by pile-up.

2.5.3. AXP CXOU J164710.2–455216

We analyzed the short burst from AXP CXOU J164710.2–455216 (Krimm et al. 2006). We generated the burst spectrum using the *Swift* BAT data from $t = 0.0585$ s to $t = 0.0725$ s, where $t = 0$ indicates the trigger time. Since reliable kT_{LT} and R_{LT} could not be obtained by 2BB, BB was used (table 12).

The post-burst emission was observed 15 times by *Swift* XRT from 2006 to 2007. We performed the joint spectral analyses using the data in both WT and PC modes for four observations, and their spectra were well reproduced

by 2BB (table 12). On the other hand, the spectra of the other 12 observations were fitted by BB (table 12), because reliable kT_{LT} and R_{LT} could not be achieved by 2BB.

The quiescent emission was observed at 7 epochs by *Chandra* from 2005 to 2007. The observations were performed before the short burst, while the other 5 observations were performed after it. The two pre-burst observations (table 5) were utilized, because the post-burst observations were performed in timing mode. The spectral analyses by BB gave a rather large reduced χ^2 which were consistent with Muno et al. (2006). The spectral analyses were improved using 2BB, but a reliable kT_{HT} could not be obtained. In table 11, we report the results of the spectral analyses by BB.

Although the quiescent emission of the post-burst was observed at one epoch by *Suzaku* in 2006 (Naik et al. 2008), we did not utilize this data in our study. The two follow-up observations by XMM-Newton were not utilized, because they were not archived at this point.

Figure 1 shows a time history of the spectral parameters obtained by the *Swift* XRT data and the flux is decaying in time.

2.5.4. AXP 1RXS J170849.0–400910

AXP 1RXS J170849.0–400910 was observed at one epoch by XMM-Newton in 2003 (table 4). Since pile-up for the MOS1 and MOS2 cameras was significant, only the pn camera data was utilized. The spectrum was not reproduced by a 2BB ($\chi^2/\text{d.o.f.} = 1566/1232$), there seemed to be an excess above ~ 7 keV (table 10), similar to AXP 4U 0142+614 (see subsection 2.5.2).

2.5.5. AXP 1E 1841–045

AXP 1E 1841–045 was observed at two epochs by XMM-Newton in 2002 (table 4). The spectra were well reproduced by 2BB (table 10).

This object was also observed by *Chandra* in 2000 and the detailed spectral analyses with 2BB were reported by Morii et al. (2003). Therefore we did not utilize this observation.

2.5.6. AXP 1E 2259+586

AXP 1E 2259+586 was observed at 6 epochs by XMM-Newton from 2002 to 2005. We just utilized three observations by the pn camera (table 4), because the other observations were affected by a photon pile-up effect. The spectra were not reproduced by 2BB for two observations ($\chi^2/\text{d.o.f.} = 1167/888$ and $\chi^2/\text{d.o.f.} = 1531/1053$), there seemed to be an excess above ~ 7 keV (table 10). These results are the same as those of AXPs 4U 0142+614 and 1RXS J170849.0–400910 (see subsections 2.5.2 and 2.5.4). Note that the spectrum of one observation on 2005 July 28 was well reproduced by 2BB ($\chi^2/\text{d.o.f.} = 457/458$ in table 10) in spite of a small net exposure time (2.66 ks).

This object was also observed at two epochs by *Chandra* in 2000 and 2006. These observations were not utilized in our study, because one observation on 2000 January 12 was affected by pile-up (Patel et al. 2001) and the other observation on 2006 May 9 was not archived at this point.

3. Discussions

3.1. Two Possible Spectral Models for Quiescent Emission

Quiescent emission spectra of the AXPs were used to examine the blackbody plus power law model (BB+PL). Recent studies suggested that the quiescent emission spectra of the SGRs and AXPs are reproduced by either a two blackbody function (2BB) or a BB+PL. To compare 2BB and BB+PL, spectral fits for one SGR 1806–20 observation (0205350101) and one AXP 4U 0142+614 observation (0112781101) were performed using these two spectral models. For SGR 1806–20, a spectral fit with 2BB gives $\chi^2/\text{d.o.f.} = 2244/2224$ with $P = 0.38$, while a spectral fit with BB+PL gives $\chi^2/\text{d.o.f.} = 2274/2224$ with $P = 0.23$. Here, P denotes a null hypothesis probability. For AXP 4U 0142+614, a spectral fit with 2BB gives $\chi^2/\text{d.o.f.} = 1086/819$ with $P = 10^{-10}$, while a spectral fit with BB+PL gives $\chi^2/\text{d.o.f.} = 978/819$ with $P = 10^{-5}$. In this case, both spectral models are rejected. These three datasets have all good statistics, therefore these acceptability and unacceptability of the fits are not simply due to their statistics, and may reflect complexity of spectral shape of radiations from these SGRs and AXPs. A recent study using HETE-2 data reports that the most acceptable model of SGR short burst spectra is 2BB even if it is an empirical model (Nakagawa et al. 2007). It is very interesting to investigate if the spectra of both the quiescent emission and the bursts are reproduced by same spectral model 2BB.

3.2. Spectral Parameter of Two Blackbody Function

As shown in subsection 2.4, both the spectra of the quiescent emission and short bursts were well reproduced by 2BB with some exceptions. The quiescent emission spectra of three AXPs (4U 0142+614, 1RXS J170849.0–400910 and 1E 2259+586) seemed to have an excess above ~ 7 keV (see subsection 3.3). In some cases, the spectra of the quiescent emission and short bursts were fitted with a photoelectrically absorbed single blackbody function (BB). This was just due to a low X-ray flux and/or insufficient exposure time to determine the reliable 2BB spectral parameters. Therefore we restrict our discuss to spectra that were well modeled by a 2BB model in order to investigate the global characteristic among the magnetar candidates, and between the quiescent emission and the bursts.

Figure 3 shows the relationship between lower and higher temperatures (kT_{LT} and kT_{HT}). The 2BB temperatures were obtained by our study and previous works (Morii et al. 2003; Feroci et al. 2004; Olive et al. 2004; Gotthelf et al. 2004; Gotthelf & Halpern 2005; Tiengo et al. 2005; Götz et al. 2006a; Mereghetti et al. 2006a; Nakagawa et al. 2007). The 2BB temperatures of 51 short bursts detected by HETE-2 are also plotted in figure 3 (Nakagawa et al. 2007).

In figure 3, there seems to be a strong correlation between kT_{LT} and kT_{HT} . It is remarkable that the correlation seems to be independent of the objects and/or the

emission types (the quiescent emission or the burst). In order to clarify the correlation, it is essential to consider systematic errors among the satellites. The systematic errors of fluxes between XMM-Newton and *Chandra* are reported to be 10-20% (Snowden 2002)³. Since the data of these satellites are important for the correlation, we focus our attention on the above systematic errors of 15%. The amount errors are described by $\sqrt{\sigma_1^2 + \sigma_2^2}$, where σ_1 and σ_2 are statistical and systematic errors, respectively. The $kT_{\text{LT}}-kT_{\text{HT}}$ relation was fitted with a power law model $kT_{\text{HT}} = A(kT_{\text{LT}})^\eta$, where A is a normalization and η is an index. Here, the errors on kT_{HT} were taken into account for the fitting. In the following discussions, quoted errors on all parameters are 90% confidence level. The parameters were found to be $A = 2.7 \pm 1.1$ and $\eta = 1.0 \pm 0.3$ with $\chi^2/\text{d.o.f.} = 86/92$. Interestingly, the derived index is just unity; this implies that kT_{LT} and kT_{HT} have a *linear* correlation and the ratio $kT_{\text{LT}}/kT_{\text{HT}} = 0.37 \pm 0.15$ is almost constant over 1.5 order of magnitudes. The linear correlation coefficient between kT_{LT} and kT_{HT} was $r = 0.99$. In addition, the relation was separately determined for the quiescent emission and the burst, where the parameters were $A = 2.6 \pm 0.9$ and $\eta = 1.0 \pm 0.3$ with $\chi^2/\text{d.o.f.} = 28/27$, and $A = 5.8 \pm 2.5$ and $\eta = 0.4^{+0.5}_{-0.3}$ with $\chi^2/\text{d.o.f.} = 18/63$, respectively. The linear correlation coefficient was $r = 0.97$ for both cases. The index for the quiescent emission is consistent with that for the burst within 90% confidence level. This means that kT_{LT} and kT_{HT} are very well correlated irrespective of objects and/or emission types (i.e., the quiescent emission and the bursts). Note that the fitting with the errors on kT_{LT} gave consistent results in each model fitting. It is also worth noting that the spectrum of a tentative magnetar candidate, 1E 1207–5209, was well reproduced by 2BB (De Luca et al. 2004), and the ratio $kT_{\text{LT}}/kT_{\text{HT}} = 0.514 \pm 0.004$ is marginally consistent with the ratio of the magnetar candidates.

The constant ratio $kT_{\text{LT}}/kT_{\text{HT}} \approx 0.4$ may imply that the spectra of the magnetar candidates have a similar shape, the emission radii should be considered. Indeed, there seems to be a correlation between R_{LT}^2 and R_{HT}^2 (figure 4). The 2BB radii are derived from our study and the previous works. The solid line in figure 4 shows that a ratio defined as $(R_{\text{LT}}/R_{\text{HT}})^2$ get constant value (0.01).

The linear correlations of $kT_{\text{LT}}-kT_{\text{HT}}$ and $R_{\text{LT}}^2-R_{\text{HT}}^2$ might imply that all the spectra have similar shape. In other words, there might be the same emission mechanisms among the magnetar candidates, and between the quiescent emission and the bursts even though 2BB is an empirical model. The latter is reminiscent of the relationship between frequent microflares and ordinary solar flares of the sun (Feldman et al. 1995; Shimizu 1995; Yuda et al. 1997). The microflares are dim, small scale flares, while the solar flares are bright, large scale flares. The microflares are thought to play an important role to heat the solar corona. Recently, it was revealed by *Hinode* (Ichimoto et al. 2005) that the microflares oc-

curred in the active bright regions on the surface of the sun. Considering the relationship between the microflares and the solar flares, the quiescent emissions of the magnetar candidates could be due to frequent small scale activity. On the other hand, the could be due to larger scale activity (or an avalanche like event of the small scale activity).

In figure 3, kT_{HT} of the quiescent emission for some magnetar candidates clearly exceeds ~ 2 keV. Using kT_{HT} and R_{HT} obtained from the observation of 0148210101 for SGR 1806–20, a flux of the kT_{HT} component turned out to be $F_{\text{HT}} = 4.84 \times 10^{25} (kT_{\text{HT}}/2.62 \text{ keV})^4 \text{ ergs cm}^{-2} \text{ s}^{-1}$, larger than the Eddington flux $F_{\text{Edd}} = 1.34 \times 10^{25} (M_{\text{NS}}/1.4 M_{\odot}) (R_{\text{NS}}/10 \text{ km})^{-2} \text{ ergs cm}^{-2} \text{ s}^{-1}$, where M_{NS} is the mass of the neutron star and R_{NS} is the radius of the neutron star. This implies that a radiation pressure is very strong and the plasma of the kT_{HT} component cannot exist steadily. This could be due to the combined effects of the confinement of the plasma and the strong magnetic field suppressing the motion of the particles in directions perpendicular to the field lines, thus decreasing the cross-section for Compton scattering.

One can see large emission radii of $R_{\text{LT}}^2 \gtrsim 100^2 \text{ km}$ for the bursts in figure 4. The magnetic field, B , is dramatically decreased as one moves from the center of the neutron star, R , because $B \propto R^{-3}$. The plasma of the kT_{LT} component might be diffused by radiation pressure without a magnetic field as strong as $\sim 10^{15} \text{ G}$ at $R \gtrsim 100 \text{ km}$. To investigate whether the plasma is diffused, the magnetic pressure and the radiation pressure at $R \gtrsim 100 \text{ km}$ were investigated. The magnetic pressure and the radiation pressure at an outer radius of the emission region were estimated using spectral parameters of the short burst of #3854 ($kT_{\text{LT}} = 1.7 \text{ keV}$ and $R_{\text{LT}} = 136 \text{ km}$) in Nakagawa et al. (2007). A spherical emission region was considered for the sake of simplicity. The center of the emission region was assumed to be aligned to the center of the neutron star. The magnetic pressure turns out to be $p_{\text{m}} \sim 1.6 \times 10^{21} (R/136 \text{ km})^{-6} (B_{\text{s}}/5.0 \times 10^{14} \text{ G})^2 \text{ ergs cm}^{-3}$, where B_{s} is the assumed surface dipole magnetic field at $R = 10 \text{ km}$. The radiation pressure turned out to be $p_{\text{r}} \sim 3.8 \times 10^{14} (kT/1.7 \text{ keV})^4 \text{ ergs cm}^{-3}$, where kT is a blackbody temperature of the emission region. Consequently, the plasma is not diffused by the radiation pressure because $p_{\text{m}} > p_{\text{r}}$.

Figure 5 shows the relationships between kT_{LT} and R_{LT}^2 (left), and between kT_{HT} and R_{HT}^2 (right). One may see that data points of the quiescent emission and the burst are apparently clustering in separate areas of this plot despite the linear correlations for $kT_{\text{LT}}-kT_{\text{HT}}$ and $R_{\text{LT}}^2-R_{\text{HT}}^2$. The data points seems to be distributed along the direction of two lines with same functional form in figure 5. This might imply a different origin and/or mechanism for the quiescent emission and the burst. Combining the $kT_{\text{LT}}-kT_{\text{HT}}$ and $R_{\text{LT}}^2-R_{\text{HT}}^2$ correlations, and the above mentioned speculations, the bolometric luminosity might be given by a function of kT_{LT} , kT_{HT} , R_{LT} or R_{HT} with the same indices irrespective of the emission types (i.e., the quiescent emission and the bursts). To clarify this hy-

³ The other document is available at http://cxc.harvard.edu/ccw/proceedings/04_proc/presentations/kashyap/kashyap.pdf.

pothesis, relations between the bolometric luminosity and kT_{LT} , kT_{HT} , R_{LT} or R_{HT} were investigated. We found that the index of the quiescent emission was not consistent with the index of the burst in any cases. Therefore, the apparent clustering in separate areas for the quiescent emission and the burst in figure 5 might not be real. It is obvious to consider the detectability for the burst with the instrument of wide field of view, such as the WXM on-board HETE-2, comparing to that of the narrow field of view detectors with X-ray telescopes for the quiescent emission. In figure 5, the dotted and dashed lines correspond to bolometric fluences of 10^{-8} and 10^{-9} ergs cm^{-2} , respectively. Most of the short bursts localized by the WXM/HETE-2 have fluences greater than 10^{-8} ergs cm^{-2} (Nakagawa et al. 2007). This may suggest that dim bursts ($\lesssim 10^{-8}$ ergs cm^{-2}) are not detectable by the WXM/HETE-2. Such dim bursts may fall on a gap between the burst population and the quiescent emission population.

3.3. An Excess above ~ 7 keV for Three AXPs

Soft X-ray spectra of the quiescent emission of three AXPs 1E2259+586, 4U0142+614 and 1RXSJ170849.0–400910 observed by XMM-Newton were not reproduced by 2BB in spite of enough statistics (see subsection 2.4). One can see an excess above ~ 7 keV in their spectra.

Recent studies discovered a non-thermal hard component above ~ 20 keV in the quiescent emission of the SGRs and the AXPs using data derived from INTEGRAL observations (Molkov et al. 2005; Götz et al. 2006b; Kuiper et al. 2006). The spectra of the non-thermal hard component were well reproduced by a power law model (Molkov et al. 2005; Götz et al. 2006b; Kuiper et al. 2006). Kuiper et al. (2006) reported the non-thermal hard component for the AXPs 4U0142+614 and 1RXSJ170849.0–400910, while they estimated just an upper limit for AXP 1E2259+586.

The excesses above ~ 7 keV in our data seem to be associated with the non-thermal hard component above ~ 20 keV discovered by INTEGRAL. To investigate our idea, a power law model related to the non-thermal hard component reported by Kuiper et al. (2006) was added to the 2BB and BB+PL spectral fits. A photon index and a normalization at 20 keV of the additional power law model were fixed to 1.05 and 2.3×10^{-5} photons $\text{cm}^{-2} \text{s}^{-1} \text{keV}$ for AXP 4U0142+614, and 1.44 and 8.8×10^{-6} photons $\text{cm}^{-2} \text{s}^{-1} \text{keV}$ for AXP 1RXSJ170849.0–400910 (Kuiper et al. 2006). For AXP 4U0142+614, 2BB+PL gave an acceptable result of $\chi^2/\text{d.o.f.} = 876/819$ with $P = 0.08$ while BB+2PL gave a poor result of $\chi^2/\text{d.o.f.} = 1067/819$ with $P = 1 \times 10^{-8}$. On the other hand, 2BB+PL gave a poor result of $\chi^2/\text{d.o.f.} = 1438/1232$ with $P = 4 \times 10^{-5}$ while BB+2PL gave $\chi^2/\text{d.o.f.} = 1270/1232$ with $P = 0.22$ for AXP 1RXSJ170849.0–400910. In figure 2 (a), the schematic view of a 2BB+PL spectrum for AXP 4U0142+614 is represented. The circles and squares denote observational data, while the dashed, dot-dash and dotted lines are model. For the sake of compar-

ison, the schematic view of a BB+2PL spectrum for AXP 4U0142+614 is also shown in figure 2 (b). Note that a distinctive hard component (e.g., the harder power law) is required for either case to represent non-thermal component seen by INTEGRAL separately from the higher temperature blackbody or secondary steep power law model. The non-thermal hard component can affect the low energy spectra ($\lesssim 12$ keV). The apparent disagreement between the quiescent emission spectra and 2BB for the three AXPs (1E2259+586, 4U0142+614 and 1RXSJ170849.0–400910) might be due to a narrow observational energy band (e.g., $\lesssim 12$ keV). Therefore, one must not reject 2BB just using the data of the X-ray band.

Although only the upper limit of a normalization (less than 3.3×10^{-6} photons $\text{cm}^{-2} \text{s}^{-1} \text{keV}$ at 30 keV) was reported for AXP 1E2259+586 (Kuiper et al. 2006), this upper limit was marginally consistent with a normalization estimated by our spectral analyses within the error. The non-detection of the non-thermal hard component above 20 keV for AXP 1E2259+586 by INTEGRAL (Kuiper et al. 2006) might imply that a photon index is very steep and/or there is a spectral cutoff.

To search the non-thermal hard component for AXP 1E2259+586 and also other magnetar candidates would be very important for understanding the intrinsic physics of magnetars. The detailed studies of the non-thermal hard component would be achieved by simultaneous observations by highly-sensitive detectors such as the X-ray imaging spectrometer (0.2–12 keV; Koyama et al. 2007) and the hard X-ray detector (10–700 keV; Takahashi et al. 2007) on-board *Suzaku* (Mitsuda et al. 2007).

4. Conclusions

The spectral studies using the photoelectrically absorbed two blackbody function (2BB) were presented for the quiescent emission and the burst of the magnetar candidates. The spectra of the quiescent emission were well reproduced by a 2BB with some exceptions. The spectra of three AXPs (4U0142+614, 1RXSJ170849.0–400910 and 1E2259+586) seem to have an excess which might be due to a non-thermal hard component discovered by INTEGRAL. The spectrum of the burst from the SGR candidate SGR 2013+34 was also well reproduced by 2BB.

A strong linear correlations between kT_{LT} and kT_{HT} was found using 2BB spectra. The ratio $kT_{LT}/kT_{HT} \sim 0.4$ is almost constant irrespectively of the objects and/or emission types (burst or quiescent emission). The relationship between R_{LT}^2 and R_{HT}^2 seems to have a linear correlation. Considering these correlations, there seems to be a common emission mechanism among these objects, and between the quiescent emission and the burst. The relationship between the quiescent emission and the burst might be similar to the relationship between microflares and an ordinary solar flares of the sun. The quiescent emission might be due to very frequent small activity similar to the microflares. On the other hand, the burst might be due to a relatively large activity similar to the ordinary solar flare.

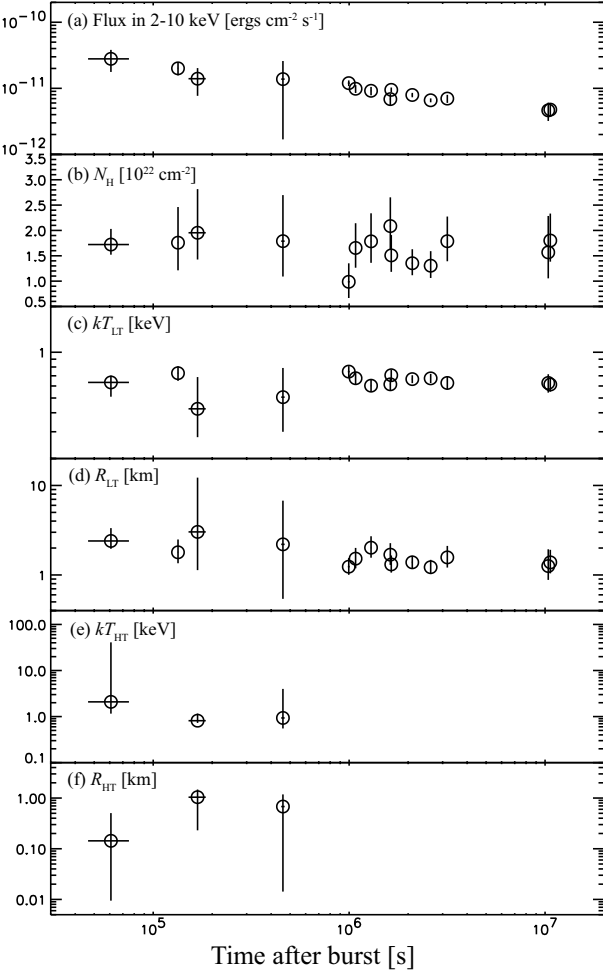


Fig. 1. Time history of the (a) flux in 2-10 keV in units of $\text{ergs cm}^{-2} \text{s}^{-1}$, (b) photoelectric absorption N_{H} in units of cm^{-2} , (c) temperature of the lower blackbody kT_{LT} in units of keV, (d) radius of the lower blackbody R_{LT} in units of km, (e) temperature of the higher blackbody kT_{HT} in units of keV and (f) radius of the higher blackbody R_{HT} in units of km for the emissions of AXP CXOU J164710.2-455216 observed by XRT/*Swift*.

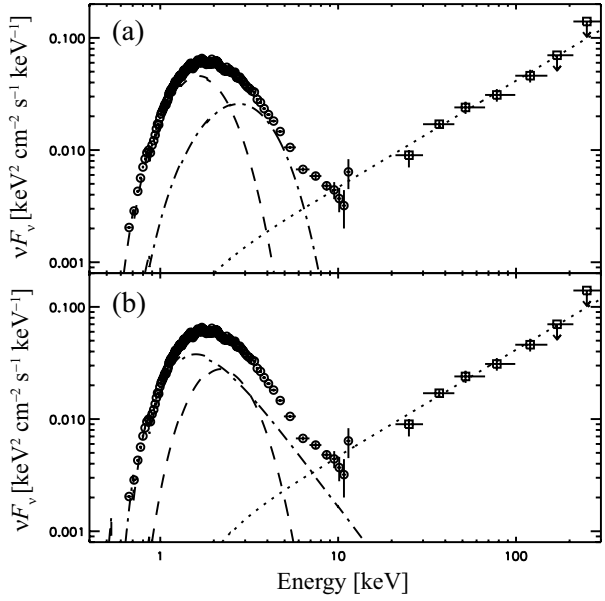


Fig. 2. A schematic view of νF_{ν} spectra using 2BB+PL (a) and BB+2PL (b) for AXP 4U 0142+614. Spectral parameters of X-ray spectra (i.e., $\lesssim 12$ keV) are derived from our analyses using the XMM-Newton observation of 0112781101, while those of the non-thermal hard component (i.e., $\gtrsim 20$ keV) is obtained by INTEGRAL observations (Kuiper et al. 2006). The circles denote data derived from our analyses using the XMM-Newton observation of 0112781101. The squares represent INTEGRAL observations taken from Fig.7 in Kuiper et al. (2006) by eye. The dashed, dot-dash, dotted lines in (a) show the kT_{LT} component, the kT_{HT} component and the PL component for the hard spectrum, respectively. Those lines in (b) show the kT component, the PL component for an X-ray spectrum and the PL component for the hard spectrum, respectively.

We would like to thank an anonymous referee for helpful comments and suggestions to improve our paper. This work is based on observations obtained with XMM-Newton, an ESA science mission with instruments and contributions directly funded by ESA Member States and NASA. We would like to thank public data archive of *Chandra*. This research has made use of software provided by the Chandra X-ray Center (CXC) in the application packages CIAO, ChIPS, and Sherpa. We acknowledge the use of public data from the Swift data archive. YEN is supported by the JSPS Research Fellowships for Young Scientists. This work is supported in part by a special postdoctoral researchers program in RIKEN.

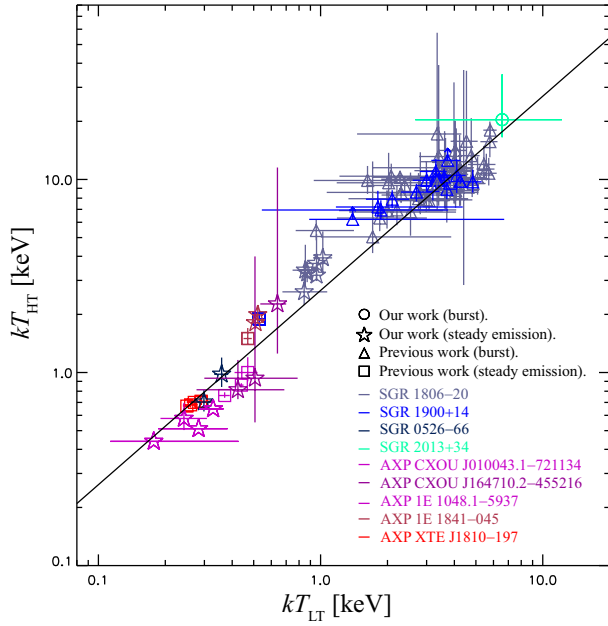


Fig. 3. Relationship between the 2BB temperatures kT_{LT} and kT_{HT} . The triangles and squares denote the previous work on the bursts (Feroci et al. 2004; Olive et al. 2004; Götz et al. 2006a; Nakagawa et al. 2007) and the quiescent emission (Morii et al. 2003; Gotthelf et al. 2004; Gotthelf & Halpern 2005; Tiengo et al. 2005; Mereghetti et al. 2006a), respectively. The circles and stars denote our work on the bursts and the quiescent emission, respectively. The line represents the best-fit power law model.

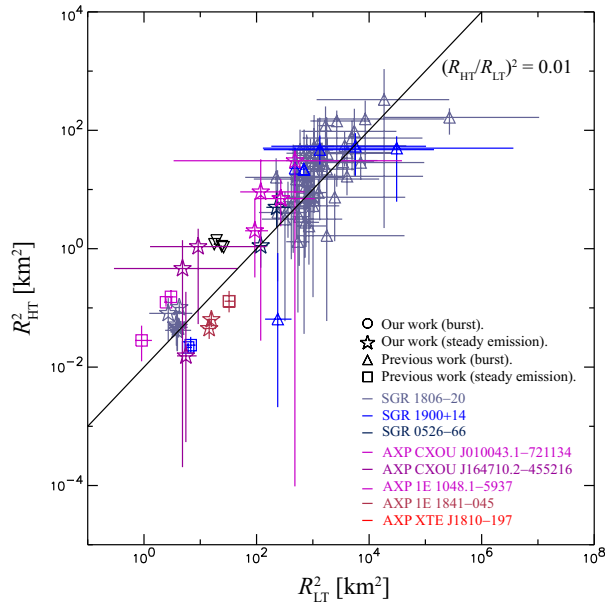


Fig. 4. Relationship between the square of the blackbody radii R_{LT}^2 and R_{HT}^2 . The triangles and squares denote the previous work on the the bursts (Olive et al. 2004; Nakagawa et al. 2007) and the quiescent emission (Morii et al. 2003; Tiengo et al. 2005; Mereghetti et al. 2006a), respectively. The stars denote our work on the quiescent emission. The solid line shows a ratio of R_{HT}^2 to R_{LT}^2 of 0.01.

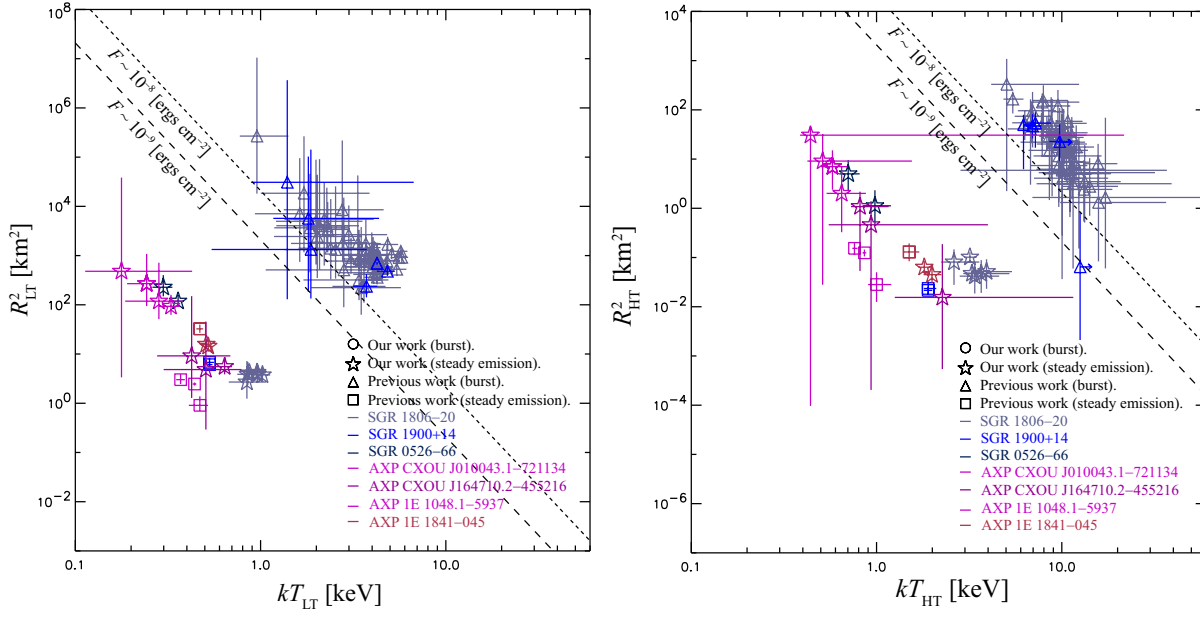


Fig. 5. *Left:* Relationship between the lower temperature of 2BB kT_{LT} and the square of the blackbody radii of 2BB R_{LT}^2 . *Right:* Relationship between the higher temperature of 2BB kT_{HT} and the square of the blackbody radii R_{HT}^2 . The dotted and dashed lines correspond to bolometric fluences of 10^{-8} and 10^{-9} ergs cm⁻², respectively.

Table 1. A summary of magnetar candidates which were employed in our study.

Object*	Satellite/Instrument [†]	Period [‡]	Distance [§]	Ref.
SGR 0526–66	<i>Chandra</i> ACIS	2000-2001	50	(1)
SGR 1627–41	XMM-Newton EPIC, <i>Chandra</i> ACIS	2001-2005	11	(2), (3), (4)
SGR 1806–20	XMM-Newton EPIC, <i>Chandra</i> ACIS	2000-2005	15 [#]	(5), (6)
SGR 2013+34	<i>Swift</i> BAT	2005	10	(7), (8)
SGR 1819–16	XMM-Newton EPIC	2003	10	
AXP CXOU J010043.1–721134	XMM-Newton EPIC, <i>Chandra</i> ACIS	2000-2005	57	(9), (10)
AXP 4U 0142+614	XMM-Newton EPIC	2002-2004	3	(11)
AXP CXOU J164710.2–455216	<i>Swift</i> BAT, <i>Swift</i> XRT, <i>Chandra</i> ACIS	2005-2007	5	(12), (13), (14), (15)
AXP 1RXS J170849.0–400910	XMM-Newton EPIC	2003	5	(16), (17)
AXP 1E 1841–045	XMM-Newton EPIC	2002	7 ^{**}	
AXP 1E 2259+586	XMM-Newton EPIC	2002-2005	3	(18)

* Object name of magnetar candidates (SGR 2013+34 denotes SGR candidate SGR/GRB 050925).

[†] Instrument and satellite names from which obtained the data used in our analysis.

[‡] Interval which these observations were performed.

[§] Distances to each object in units of kpc (see Woods & Thompson 2006 and references there in).

^{||} (1) Kurkarni et al. (2003); (2) Kouveliotou et al. (2003); (3) Wachter et al. (2004); (4) Mereghetti et al. (2006b); (5) Kaplan et al. (2002); (6) Mereghetti et al. (2005); (7) Holland et al. (2005); (8) Markwardt et al. (2005); (9) Lamb et al. (2002); (10) Majid, Lamb & Macomb (2004); (11) Güver, Özel & Göğüş (2007); (12) Krimm et al. (2006); (13) Campana & Israel (2006); (14) Munro et al. (2006); (15) Munro et al. (2007); (16) Oosterbroek et al. (2004); (17) Rea et al. (2007); (18) Woods et al. (2004)

[#] The latest distance estimate is $d = 8.7$ kpc (Bibby et al. 2008).

^{**} The latest distance estimate is $d = 8.5$ kpc (Tian & Leahy 2008).

Table 2. XMM-Newton observations of the quiescent emissions of the SGRs.

Object*	ObsID [†]	Observation Date (MJD) [‡]		Observation Mode [§]			Exposure Time (ks)			Source/Background Radii		
		Start	End	pn	MOS1	MOS2	pn	MOS1	MOS2	pn	MOS1	MOS2
1627–41	0204500201	53051.590	53051.992	Full	Full	Full	15.89	20.03	20.17	10''/10''	10''/10''	10''/10''
1627–41	0204500301	53252.750	53253.131	Full	Full	Full	27.06	32.00	32.10	10''/10''	10''/10''	10''/10''
1627–41	0202560101	53270.677	53271.281	Small	P-W2	P-W2	26.66	36.19	49.38	10''/10''	10''/10''	10''/10''
1806–20	0148210101	52732.566	52733.209	Full	P-W3	P-W3	4.84	5.65	5.62	32''/32''	28''/28''	28''/28''
1806–20	0148210401	52919.404	52919.663	Full	P-W3	P-W3	7.61	7.07	7.23	32''/32''	28''/28''	28''/28''
1806–20	0205350101	53254.377	53254.978	Small	P-W3	P-W3	30.21	39.14	39.56	32''/32''	28''/28''	28''/28''
1806–20	0164561101	53284.706	53284.925	Small	Fast-U	Fast-U	11.54	t	t	32''/32''
1806–20	0164561301	53436.348	53436.636	Small	Fast-U	Full	7.37	t	5.68	32''/32''	...	28''/28''
1806–20	0164561401	53647.427	53647.809	Small	Fast-U	Full	22.11	t	28.68	32''/32''	...	28''/28''
2013+34	0212481201	53655.026	53655.334	Full	Full	Full	22.18	25.27	25.27	32''/32''	28''/28''	28''/28''
1819–16	0152834501	52726.191	52726.310	Full	Full	Full	3.3	4.3	4.8	32''/80'' [#]	28''/70'' [#]	28''/70'' [#]

* Object name of the SGRs (2013+34 denotes SGR candidate SGR/GRB 050925 and 1819–16 denotes SGR candidate AX J1818.8–1559).

[†] XMM-Newton observation ID.

[‡] Start and end time of observations.

[§] Observation mode for each instrument; full-window mode (Full), small-window mode (Small), partial-w2 mode (P-W2), partial-w3 mode (P-W3) and fast-uncompressed mode (Fast-U).

^{||} Net exposure time for each instrument. t denotes the data sets obtained by the MOS cameras in timing mode and not utilized.

[#] The background regions were extracted from an annular region whose center was the source position. The first values are source radii, and the inner radii of the background regions. The second values are outer radii of the background regions.

Table 3. *Chandra* observations of the quiescent emissions of the SGRs.

Object*	ObsID [†]	Observation Date (MJD) [‡]		Observation Mode [§]	Exposure Time (ks)	Source/Background Radii
		Start	End			
0526–66	747	51547.017	51547.539	FAINT	39.86	1''/1''
0526–66	1957	52152.937	52153.566	FAINT	48.45	1''/1''
1627–41	1981	52182.205	52182.803	FAINT	48.93	2''/2''
1627–41	3877	52722.169	52722.494	VFAINT	25.67	2''/2''

* SGR names.

[†] *Chandra* observation ID.

[‡] Start and end time of the observations.

[§] FAINT and VFAINT denote the imaging mode, and CC33_FAINT denotes the timing mode.

^{||} Net exposure time.

Table 4. XMM-Newton observations of the quiescent emissions of the AXPs.

Object*	ObsID [†]	Observation Date (MJD) [‡]		Observation Mode [§]			Exposure Time (ks)			Source/Background Radii		
		Start	End	pn	MOS1	MOS2	pn	MOS1	MOS2	pn	MOS1	MOS2
0100–721	0110000201	51834.626	51834.867	E-Full	Full	Full	20.81	14.62	<i>g</i>	32''/32''	28''/28''	28''/28''
0100–721	0018540101	52233.983	52234.303	Full	Full	Full	21.16	25.73	<i>g</i>	32''/32''	28''/28''	28''/28''
0142+614	0112781101	52663.920	52663.995	Small	Fast-U	Fast-U	4.18	<i>t</i>	<i>t</i>	32''/32''
1708–400	0148690101	52879.906	52880.426	Full	P-W3	P-W3	26.88	<i>p</i>	<i>p</i>	20''/20''
1841–045	0013340101	52552.122	52552.192	Large	Full	Full	2.34	3.54	3.57	12''/12''	12''/12''	12''/12''
1841–045	0013340201	52554.115	52554.193	Large	Full	Full	4.37	6.30	6.30	12''/12''	12''/12''	12''/12''
2259+586	0038140101	52436.378	52436.986	Small	Full	Full	30.63	<i>p</i>	<i>p</i>	32''/32''
2259+586	0155350301	52446.400	52446.759	Small	P-W2	Full	17.65	<i>p</i>	<i>p</i>	32''/32''
2259+586	0203550701	53579.965	53580.030	Small	P-W2	Fast-U	2.66	<i>p</i>	<i>t</i>	32''/32''

* Object name of the AXPs; CXOU J010043.1–721134 (0100–721), 4U 0142+614 (0142+614), 1RXS J170849.0–400910 (1708–400), 1E 1841–045 and 1E 2259+586.

[†] XMM-Newton observation ID.

[‡] Start and end time of the observations.

[§] Observation mode for each instrument; extended full-window mode (E-Full), Full-window mode (Full), small-window mode (Small), fast-uncompressed mode (Fast-U), fast-timing mode (Fast-T), partial-w3 mode (P-W3), large-window mode (Large) and partial-w2 mode (P-W2).

^{||} Net exposure time for each instrument. *g* denotes that the source fell on a gap of the CCD chips, *t* denotes observations in timing mode, and *p* denotes that the data sets are affected by a photon pile-up. These data sets were not utilized.

Table 5. *Chandra* observations of the quiescent emissions of the AXPs.

Object*	ObsID [†]	Observation Date (MJD) [‡]		Observation Mode [§]	Exposure Time (ks)	Source/Background Radii
		Start	End			
0100–721	1881	52044.080	52045.261	FAINT	98.67	11''/10'' [#]
0100–721	4616	53031.791	53032.009	VFAINT	15.56	2''/2''
0100–721	4617	53032.189	53032.399	VFAINT	15.27	2''/2''
0100–721	4618	53033.904	53034.130	VFAINT	15.00	2''/2''
0100–721	4619	53042.806	53043.023	VFAINT	15.04	2''/2''
0100–721	4620	53089.185	53089.395	VFAINT	15.22	2''/2''
1647–455	6283	53512.860	53513.102	FAINT	18.81	2''/2''
1647–455	5411	53539.673	53540.141	FAINT	38.47	2''/2''

* Object name of the AXPs; CXOU J010043.1–721134 (0100–721) and CXOU J164710.2–455216 (1647–455).

[†] *Chandra* observation ID.

[‡] Start and end time of observations.

[§] FAINT and VFAINT denote the imaging mode.

^{||} Net exposure time.

[#] Since the source fell on an off-axis CCD chip, the source region was extracted from an elliptical region with major and minor axes of 11'' and 10'', respectively.

Table 6. *Swift* observations of the quiescent emission and the bursts of AXP CXOU J164710.2–455216.

SeqNum*	Observation Date (MJD) [†]		Start (PC)		End (PC)		Exposure Time (ks) [‡]		Source/Background Radii	
	Start (WT)	End (WT)	Start (PC)	End (PC)	WT	PC	WT	PC		
00230341000 [§]	
00030806001	53999.604	53999.924	53999.604	53999.936	1.92	7.74	36'' × 18''/36'' × 18''	30''/30''		
00030806002	54000.610	54000.619	0.77	...	36'' × 18''/36'' × 18''	...		
00030806003	54000.819	54001.212	54000.819	54001.073	4.91	1.84	36'' × 18''/36'' × 18''	30''/30''		
00030806004	54004.276	54004.483	54004.343	54004.489	1.25	2.48	36'' × 18''/36'' × 18''	30''/30''		
00030806006	54010.461	54010.716	1.98	...	36'' × 18''/36'' × 18''	...		
00030806007	54011.515	54011.594	2.03	...	36'' × 18''/36'' × 18''	...		
00030806008	54014.001	54014.077	2.16	...	36'' × 18''/36'' × 18''	...		
00030806009	54017.746	54017.954	3.52	...	36'' × 18''/36'' × 18''	...		
00030806010	54018.009	54018.094	2.83	...	36'' × 18''/36'' × 18''	...		
00030806011	54023.237	54023.517	5.62	...	36'' × 18''/36'' × 18''	...		
00030806012	54029.125	54029.342	5.52	...	36'' × 18''/36'' × 18''	...		
00030806013	54035.677	54035.825	54035.678	54035.774	2.82	0.42	36'' × 18''/36'' × 18''	30''/30''		
00030806014	54119.174	54119.253	2.06	...	36'' × 18''/36'' × 18''	...		
00030806015	54122.050	54122.267	3.82	...	36'' × 18''/36'' × 18''	...		

* *Swift* sequence number.[†] Start and end time of the observations for each mode (WT denotes window timing mode, and PC denotes photon counting mode).[‡] Net exposure time for each observation mode.[§] The observation of a burst.^{||} The source and background regions were extracted from a rectangle region. Two background regions are utilized near both sides of the source region.**Table 7.** Spectral parameters of the quiescent emissions of the SGRs observed by XMM-Newton.

Object*	ObsID [†]	N_{H}^{\ddagger}	kT_{LT}^{\S}	$R_{\text{LT}}^{\parallel}$	kT_{HT}^{\S}	$R_{\text{HT}}^{\parallel}$	$F^{\#}$	χ^2 (d.o.f.)
		(10^{22} cm^{-2})	(keV)	(km)	(keV)	(km)		
1627–41	0204500201	$15.98^{+15.51}_{-7.60}$	$0.58^{+0.35}_{-0.25}$	<19.25	~ 0.05	44 (42)
1627–41	0204500301	$7.53^{+6.19}_{-3.56}$	$0.85^{+0.29}_{-0.22}$	<0.62	0.08 ± 0.06	29 (65)
1627–41	0202560101	$9.00^{+6.71}_{-3.89}$	$0.94^{+0.31}_{-0.24}$	<0.42	0.06 ± 0.04	54 (47)
1806–20	0148210101	$5.18^{+0.92}_{-0.73}$	$0.84^{+0.23}_{-0.17}$	$1.64^{+1.04}_{-0.53}$	$2.62^{+0.97}_{-0.38}$	$0.28^{+0.10}_{-0.12}$	11.05 ± 1.92	312 (295)
1806–20	0148210401	$5.87^{+0.63}_{-0.55}$	$0.85^{+0.12}_{-0.11}$	$1.97^{+0.65}_{-0.43}$	$3.39^{+1.2}_{-0.58}$	0.20 ± 0.07	12.29 ± 2.4	506 (459)
1806–20	0205350101	$5.75^{+0.20}_{-0.19}$	0.96 ± 0.05	$2.06^{+0.20}_{-0.17}$	$3.19^{+0.28}_{-0.21}$	0.32 ± 0.04	25.43 ± 0.52	2243 (2224)
1806–20	0164561101	$5.43^{+0.39}_{-0.35}$	1.02 ± 0.1	$1.94^{+0.37}_{-0.27}$	$3.92^{+1.46}_{-0.69}$	0.23 ± 0.08	24.65 ± 2.74	737 (741)
1806–20	0164561301	$5.64^{+0.50}_{-0.43}$	0.96 ± 0.1	$1.98^{+0.46}_{-0.33}$	$3.67^{+1.54}_{-0.68}$	0.22 ± 0.08	18.91 ± 4.21	654 (531)
1806–20	0164561401	$5.91^{+0.34}_{-0.31}$	0.87 ± 0.06	$2.03^{+0.31}_{-0.25}$	$3.27^{+0.48}_{-0.34}$	0.22 ± 0.04	13.30 ± 0.5	1026 (1069)
2013+34	0212481201	$0.29^{+0.15}_{-0.13}$	$0.13^{+0.02}_{-0.02}$	<7.54	20.78 ± 20.12	57 (64)
1819–16	0152834501	$1.6^{+0.7}_{-0.5}$	$1.9^{+0.3}_{-0.2}$	$0.11^{+0.03}_{-0.02}$	1.3 ± 0.1	59 (74)

* Object name of the SGRs (2013+34 denotes a SGR candidate SGR/GRB 050925).

[†] XMM-Newton observation ID.[‡] N_{H} denotes the column density with 90 % confidence level errors.[§] kT_{LT} and kT_{HT} denote the blackbody temperatures with 90 % confidence level errors.^{||} R_{LT} and R_{HT} denote the emission radii with 90 % confidence level errors.[#] F denotes a flux in the energy range 2–10 keV in units of $10^{-12} \text{ ergs cm}^{-2} \text{ s}^{-1}$ with 68 % confidence level errors.

Table 8. Spectral parameters of the quiescent emissions of the SGRs observed by *Chandra*.

Object*	ObsID [†]	N_{H}^{\ddagger} (10^{22} cm $^{-2}$)	kT_{LT}^{\S} (keV)	$R_{\text{LT}}^{\parallel}$ (km)	kT_{HT}^{\S} (keV)	$R_{\text{HT}}^{\parallel}$ (km)	$F^{\#}$	χ^2 (d.o.f.)
0526–66	747	$0.20^{+0.03}_{-0.02}$	0.36 ± 0.03	$10.87^{+1.66}_{-1.26}$	$0.98^{+0.22}_{-0.14}$	$1.06^{+0.46}_{-0.37}$	0.49 ± 0.06	180 (181)
0526–66	1957	$0.26^{+0.05}_{-0.04}$	0.30 ± 0.04	$15.08^{+4.93}_{-2.87}$	$0.70^{+0.11}_{-0.07}$	$2.24^{+0.85}_{-0.72}$	0.39 ± 0.06	176 (185)
1627–41	1981	$8.47^{+6.41}_{-4.86}$	$0.89^{+0.57}_{-0.28}$	< 0.67	< 0.07	36 (34)
1627–41	3877	$17.34^{+9.89}_{-7.36}$	$0.42^{+0.2}_{-0.13}$	$3.56^{+33.39}_{-2.99}$	< 0.06	22 (21)

* Object name of the SGRs.

[†] *Chandra* observation ID.[‡] N_{H} denotes the column density with 90 % confidence level errors.[§] kT_{LT} and kT_{HT} denote the blackbody temperatures with 90 % confidence level errors.^{||} R_{LT} and R_{HT} denote the emission radii with 90 % confidence level errors.[#] F denotes the flux in the 2-10 keV band in units of 10^{-12} ergs cm $^{-2}$ s $^{-1}$ with 68 % confidence level errors.**Table 9.** Spectral parameters of a burst of SGR 2013+34 (GRB/SGR 050925) observed by *Swift*.

SeqNum*	N_{H}^{\ddagger} (10^{22} cm $^{-2}$)	$kT_{\text{LT}}^{\ddagger}$ (keV)	R_{LT}^{\S} (km)	$kT_{\text{HT}}^{\ddagger}$ (keV)	R_{HT}^{\S} (km)	F^{\parallel}	χ^2 (d.o.f.)
00156838000	...	$6.6^{+5.6}_{-3.9}$	$3.1^{+3.7}_{-1.7}$	20^{+15}_{-4}	$\gtrsim 0.2$	0.81 ± 0.28	27 (25)

* *Swift* sequence number.[†] N_{H} denotes the column density with 90 % confidence level errors.[‡] kT_{LT} and kT_{HT} denote the blackbody temperatures with 90 % confidence level errors.[§] R_{LT} and R_{HT} denote the emission radii with 90 % confidence level errors.^{||} F denotes a flux in the energy range 15-150 keV in units of 10^{-6} ergs cm $^{-2}$ s $^{-1}$ with 68 % confidence level errors.**Table 10.** Spectral parameters of the quiescent emissions of the AXPs observed by XMM-Newton.

Object*	ObsID [†]	N_{H}^{\ddagger} (10^{22} cm $^{-2}$)	kT_{LT}^{\S} (keV)	$R_{\text{LT}}^{\parallel}$ (km)	kT_{HT}^{\S} (keV)	$R_{\text{HT}}^{\parallel}$ (km)	$F^{\#}$	χ^2 (d.o.f.)
0100–721	0110000201	$\lesssim 0.06$	0.39 ± 0.02	$6.94^{+1.09}_{-0.67}$	0.09 ± 0.01	264 (275)
0100–721	0018540101	$\lesssim 0.15$	0.29 ± 0.06	$11.64^{+7.47}_{-3.35}$	$0.64^{+0.25}_{-0.11}$	$1.86^{+1.17}_{-1.08}$	0.13 ± 0.09	97 (129)
0142+614	0112781101	0.53 ± 0.01	0.36 ± 0.01	$9.38^{+0.34}_{-0.31}$	$0.82^{+0.03}_{-0.02}$	$0.89^{+0.09}_{-0.08}$	57.26 ± 0.61	1086 (819)
1708–400	0148690101	0.95 ± 0.01	0.48 ± 0.01	$4.46^{+0.11}_{-0.10}$	1.49 ± 0.04	0.29 ± 0.02	$27.42^{+0.08}_{-0.13}$	1566 (1232)
1841–045	0013340101	$1.86^{+0.14}_{-0.13}$	0.52 ± 0.03	$3.79^{+0.57}_{-0.46}$	$1.99^{+0.25}_{-0.20}$	$0.21^{+0.05}_{-0.04}$	17.39 ± 0.83	408 (391)
1841–045	0013340201	1.90 ± 0.11	0.51 ± 0.02	$3.97^{+0.48}_{-0.40}$	$1.81^{+0.14}_{-0.12}$	$0.25^{+0.04}_{-0.03}$	17.16 ± 0.51	583 (641)
2259+586	0038140101	0.59 ± 0.01	$0.353^{+0.005}_{-0.004}$	$4.88^{+0.15}_{-0.13}$	0.75 ± 0.02	$0.50^{+0.03}_{-0.04}$	12.34 ± 0.07	1167 (888)
2259+586	0155350301	0.54 ± 0.01	0.390 ± 0.006	$5.01^{+0.15}_{-0.14}$	0.85 ± 0.02	$0.67^{+0.05}_{-0.04}$	33.01 ± 0.21	1531 (1053)
2259+586	0203550701	0.59 ± 0.03	$0.356^{+0.013}_{-0.015}$	$4.97^{+0.47}_{-0.39}$	$0.82^{+0.08}_{-0.07}$	$0.43^{+0.13}_{-0.10}$	$13.77^{+0.44}_{-0.44}$	457 (458)

* Object name of the AXPs; CXOU J010043.1–721134 (0100–721), 4U 0142+614 (0142+614), 1RXS J170849.0–400910 (1708–400), 1E 1841–045 and 1E 2259+586.

[†] XMM-Newton observation ID.[‡] N_{H} denotes the column density with 90 % confidence level errors.[§] kT_{LT} and kT_{HT} denote the blackbody temperatures with 90 % confidence level errors.^{||} R_{LT} and R_{HT} denote the emission radii with 90 % confidence level errors.[#] F denotes a flux in the energy range 2-10 keV in units of 10^{-12} ergs cm $^{-2}$ s $^{-1}$ with 68 % confidence level errors.

Table 11. Spectral parameters of the quiescent emissions of the AXPs observed by *Chandra*.

Object*	ObsID [†]	N_{H}^{\ddagger} (10^{22} cm $^{-2}$)	kT_{LT}^{\S} (keV)	$R_{\text{LT}}^{\parallel}$ (km)	kT_{HT}^{\S} (keV)	$R_{\text{HT}}^{\parallel}$ (km)	$F^{\#}$	χ^2 (d.o.f.)
0100–721	1881	$0.06^{+0.06}_{-0.05}$	$0.33^{+0.04}_{-0.04}$	$9.65^{+2.98}_{-1.74}$	$0.65^{+0.23}_{-0.11}$	$1.42^{+1.25}_{-0.85}$	$0.12^{+0.05}_{-0.05}$	172 (150)
0100–721	4616	< 0.04	0.39 ± 0.02	$6.84^{+1.06}_{-0.56}$	0.09 ± 0.01	63 (68)
0100–721	4617	< 0.41	$0.18^{+0.25}_{-0.06}$	$21.90^{+173.99}_{-20.07}$	$0.44^{+21.23}_{-0.05}$	$5.53^{+1.24}_{-5.52}$	0.12 ± 0.04	66 (64)
0100–721	4618	< 0.18	0.28 ± 0.1	$10.88^{+15.89}_{-3.73}$	$0.51^{+1.04}_{-0.09}$	$3.02^{+2.67}_{-2.85}$	0.10 ± 0.09	50 (65)
0100–721	4619	< 0.04	$0.41^{+0.02}_{-0.2}$	$6.40^{+0.88}_{-0.51}$	0.11 ± 0.01	47 (67)
0100–721	4620	< 0.03	$0.40^{+0.01}_{-0.02}$	$6.67^{+0.79}_{-0.41}$	0.10 ± 0.01	70 (68)
1647–455	6283	$2.54^{+0.81}_{-0.69}$	0.49 ± 0.06	$0.52^{+0.31}_{-0.18}$	0.15 ± 0.04	23 (21)
1647–455	5411	$1.44^{+0.32}_{-0.28}$	0.58 ± 0.05	$0.26^{+0.07}_{-0.05}$	0.13 ± 0.01	54 (44)

* Object name of the AXPs; CXOU J010043.1–721134 (0100–721) and CXOU J164710.2–455216 (1647–455).

[†] *Chandra* observation ID.

[‡] N_{H} denotes the column density with 90 % confidence level errors.

[§] kT_{LT} and kT_{HT} denote the blackbody temperatures with 90 % confidence level errors.

^{||} R_{LT} and R_{HT} denote the emission radii with 90 % confidence level errors.

[#] F denotes a flux in the energy range 2-10 keV in units of 10^{-12} ergs cm $^{-2}$ s $^{-1}$ with 68 % confidence level errors.

Table 12. Spectral parameters of the quiescent emission and the bursts of AXP CXOU J164710.2–455216 observed by *Swift*.

SeqNum*	N_{H}^{\ddagger} (10^{22} cm $^{-2}$)	$kT_{\text{LT}}^{\ddagger}$ (keV)	R_{LT}^{\S} (km)	$kT_{\text{HT}}^{\ddagger}$ (keV)	R_{HT}^{\S} (km)	F^{\parallel}	χ^2 (d.o.f.)
00230341000 [#]	$8.92^{+1.34}_{-1.62}$	$1.21^{+0.59}_{-0.35}$	0.35 ± 0.12	8 (12)
00030806001	$1.72^{+0.31}_{-0.20}$	$0.63^{+0.07}_{-0.12}$	$2.40^{+0.94}_{-0.44}$	$2.08^{+38.74}_{-0.93}$	$0.14^{+0.36}_{-0.13}$	27.94 ± 10.25	253 (242)
00030806002	$1.76^{+0.70}_{-0.55}$	$0.73^{+0.08}_{-0.08}$	$1.79^{+0.7}_{-0.44}$	20.01 ± 4.36	16 (17)
00030806003	$1.95^{+0.86}_{-0.53}$	$0.42^{+0.26}_{-0.15}$	$3.03^{+9.21}_{-1.9}$	$0.81^{+0.35}_{-0.09}$	$1.04^{+0.43}_{-0.81}$	13.98 ± 6.28	101 (92)
00030806004	$1.79^{+0.91}_{-0.7}$	$0.51^{+0.28}_{-0.21}$	$2.20^{+4.56}_{-1.66}$	$0.93^{+3.06}_{-0.38}$	$0.68^{+0.5}_{-0.67}$	13.79 ± 12.1	91 (74)
00030806006	$0.99^{+0.37}_{-0.32}$	0.75 ± 0.06	$1.24^{+0.31}_{-0.23}$	11.99 ± 1.2	31 (33)
00030806007	$1.65^{+0.49}_{-0.39}$	$0.67^{+0.07}_{-0.06}$	$1.52^{+0.48}_{-0.33}$	9.85 ± 1.34	27 (29)
00030806008	$1.78^{+0.55}_{-0.42}$	0.60 ± 0.05	$2.02^{+0.69}_{-0.46}$	9.18 ± 1.33	73 (64)
00030806009	$2.09^{+0.57}_{-0.46}$	0.62 ± 0.06	$1.69^{+0.58}_{-0.39}$	6.86 ± 1.38	64 (55)
00030806010	$1.51^{+0.4}_{-0.32}$	0.71 ± 0.06	$1.31^{+0.34}_{-0.25}$	9.48 ± 0.81	47 (59)
00030806011	$1.35^{+0.28}_{-0.24}$	0.67 ± 0.04	$1.38^{+0.26}_{-0.20}$	7.93 ± 0.61	90 (93)
00030806012	$1.30^{+0.29}_{-0.24}$	0.67 ± 0.05	$1.22^{+0.25}_{-0.20}$	6.60 ± 0.45	66 (75)
00030806013	$1.79^{+0.49}_{-0.40}$	0.63 ± 0.06	$1.57^{+0.54}_{-0.36}$	7.00 ± 0.97	63 (70)
00030806014	$1.57^{+0.72}_{-0.51}$	0.63 ± 0.09	$1.26^{+0.68}_{-0.38}$	4.64 ± 1.43	22 (31)
00030806015	$1.80^{+0.53}_{-0.42}$	$0.61^{+0.07}_{-0.06}$	$1.38^{+0.53}_{-0.34}$	4.77 ± 0.84	49 (47)

* *Swift* sequence number.

[†] N_{H} denotes the column density with 90 % confidence level errors.

[‡] kT_{LT} and kT_{HT} denote the blackbody temperatures with 90 % confidence level errors.

[§] R_{LT} and R_{HT} denote the emission radii with 90 % confidence level errors.

^{||} F denotes fluxes in the energy ranges 15-150 keV in units of 10^{-6} ergs cm $^{-2}$ s $^{-1}$ for the burst observation of 00230341000 and 2-10 keV in units of 10^{-12} ergs cm $^{-2}$ s $^{-1}$ for other observations with 68 % confidence level errors.

[#] Results for the burst.

References

- Arnaud, K. A. 1996, in *Astronomical Data Analysis Software and Systems V*, ed. G. Jacoby and J. Barnes, ASP Conference Series (San Francisco: The Astronomical Society of the Pacific), 101, 17
- Barthelmy, S. D., et al. 2005, *Space Sci. Rev.*, 120, 143
- Barthelmy, S. D., et al. 2008, *GRB Coord. Netw. Circ.*, 8113
- Beardmore, A. P., et al. 2005, *GRB Coord. Netw. Circ.*, 4043
- Bibby, J. L. et al. 2008, *MNRAS*, 386, L23
- Burrows, D. N., et al. 2005, *Space Sci. Rev.*, 120, 165
- Campana S., & Israel G. L. 2006, *The Astronomer's Telegram*, 893
- Capalbi, M., Perri, M., Saija, B., Tamburelli, F., & Angelini, L. 2005, *The SWIFT XRT Data Reduction Guide*, Version 1.2, 28
- Cameron, P. B. et al. 2005, *Nature*, 434, 1112
- Cea, P. 2006, *A&A*, 450, 199
- Cline, T. et al. 1980, *ApJ*, 237, L1
- Cline, T., Fredericks, D. D., Golenetskii, S., Hurley, K., Kouveliotou, C., Mazets, M., & Van Paradijs, J. 2000, *ApJ*, 531, 407
- De Luca, A., Merethetti, S., Caraveo, P. A., Moroni, M., Mignani, R. P., & Bignami, G. F. 2004, *A&A*, 418, 625
- De Luca, A., Caraveo, P., Esposito, P., Mereghetti, S., & Tiengo A. 2005, *GRB Coord. Netw. Circ.*, 4274
- Dib, R., Kaspi, V. M., Gavriil, F. P., & Woods, P. M. 2008, *The Astronomer's Telegram*, 1769
- Duncan, R., & Thompson, C. 1992, *ApJ*, 392, L9
- Evans, W. D. et al. 1980, *ApJ*, 237, L7
- Fahlman, G. G., & Gregory, P. C. 1981, *Nature*, 293, 202
- Fahlman, G. G., & Gregory, P. C. 1983, in *Supernova Remnants and Their X-Ray Emission*, ed. J. Danziger & P. Gorenstein (Boston: D. Reidel Pub. Co.), 445
- Feldman, U., Laming, J. M., & Doschek, G. A. 1995, *ApJL*, 451, L79
- Fenimore, E. E., Evans, W. D., Klebesadel, R. W., Laros, J. G., & Terrell, J. 1981, *Nature*, 289, 42
- Fenimore, E. E., Klebesadel, R. W., & Laros, J. G. 1996, *ApJ*, 460, 964
- Feroci, M., Frontera, F., Costa, E., Amati, L., Tavani, M., Rapisarda, M., & Orlandini, M. 1999, *ApJ*, 515, L9
- Feroci, M., Hurley, K., Duncan, R. C., & Thompson, C. 2001, *ApJ*, 549, 1021
- Feroci, M., Caliendo, G. A., Massaro, E., Mereghetti, S., & Woods, P. M. 2004, *ApJ*, 612, 408
- Gaensler, B. M., et al. 2005, *Nature*, 434, 1104
- Gelfand, J., & Gaensler, B. M. 2007, arXiv: astro-ph/0706.1054
- Gavriil, F. P., Kaspi, M., & Woods, P. M. 2004, *ApJ*, 607, 959
- Gavriil, F. P., Kaspi, V. M., & Woods, P. M. 2006, *ApJ*, 641, 418
- Giacani, E. B., Dubner, G. M., Green, A. J., Goss, W. M., & Gaensler, B. M. 2000, *ApJ*, 119, 281
- Gehrels, N. et al. 2004, *ApJ*, 611, 1005
- Göhler, E., Wilms, J., & Staubert, R. 2005, *A&A*, 433, 1079
- Gonzalez, M. E., & Safi-Harb, S. 2003, *ApJ*, 591, L143
- Gonzalez, M. E., Kaspi, V. M., Lyne, A. G., & Pivovarov, M. J. 2004, *ApJ*, 610, L37
- Gotthelf, E. V., & Vasisht, G. 1998, *NewA*, 3, 293
- Gotthelf, E. V., Gavriil, F. P., Kaspi, V. M., Vasisht, G., & Chakrabarty, D. 2002, *ApJ*, 564, L31
- Gotthelf, E. V., Halpern, J. P., Buxton, M., & Bailyn, C. 2004, *ApJ*, 605, 368
- Gotthelf, E. V., & Halpern, J. P. 2005, *ApJ*, 632, 1075
- Gotthelf, E. V., & Halpern, J. P. 2007, *Ap&SS*, 308, 79
- Götz, D., et al. 2006a, *A&A*, 445, 313
- Götz, D., Mereghetti, S., Tiengo, A., & Esposito, P. 2006b, *A&A*, 449, L31
- Güver, T., Özel, F., & Göğüş, E. 2007, arXiv: astro-ph/0705.3982
- Güver, T., Özel, F., Göğüş, E., & Kouveliotou, C. 2007, arXiv: astro-ph/0705.3713
- Harding, A. K., Contopoulos, I., & Kazanas, D. 1999, *ApJ*, 525, L125
- Halpern, J. P., & Gotthelf, E. V. 2005, *ApJ*, 618, 874
- Hobbs, G., et al. 2004, *MNRAS*, 352, 1439
- Holland, S. T., Barthelmy, S., Beardmore, A., Gehrels, N., Kennea, J., Page, K., Palmer, D., & Rosen, S. 2005, *GRB Coord. Netw. Circ.*, 4034
- Hurley, K., et al. 1999a, *ApJ*, 510, L111
- Hurley, K., et al. 1999b, *Nature*, 397, 41
- Hurley, K., et al. 2005, *Nature*, 434, 1098
- Ibrahim, A. I., et al. 2004, *ApJ*, 609, L21
- Ichimoto, K., et al. 2005, *Journal of the Korean Astronomical Society*, 38, 307
- Israel, G. L., Mereghetti, S., & Stella, L. 1994, *ApJ*, 433, L25
- Israel, G. L., Dall'Osso, S., Campana, S., Munro, M., & Stella, L. 2006, *The Astronomer's Telegram*, 893
- Jansen, F., et al. 2001, *A&A*, 365, L1
- Kaplan, D. L., Fox, D. W., Kulkarni, S. R., Gotthelf, E. V., Vasisht, G., & Frail, D. A. 2002, *ApJ*, 564, 935
- Kaspi, V. M., & McLaughlin, M. A. 2005, *ApJ*, 618, L41
- Koyama, K., et al. 2007, *PASJ*, 59, S23
- Krimm, H., et al. 2006, *GRB Coord. Netw. Circ.*, 5581
- Kuiper, L., Hermsen, W., Den Hartog, P. R., & Collmar, W. 2006, *ApJ*, 645, 556
- Kurkarni, S. R., Kaplan, D. L., Marshall, H. L., Frail, D. A., Murakami, T., & Yonetoku, D. 2003, *ApJ*, 585, 948
- Kouveliotou, C., et al. 2003, *ApJ*, 596, L79
- Lamb, R. C., & Markert, T. H. 1981, *ApJ*, 244, 94
- Lamb, R. C., Fox, D. W., Macomb, D. J., & Prince, T. A. 2002, *ApJ*, 574, L29
- Lamb, D. Q., et al. 2003, *GRB Coord. Netw. Circ.*, 2351
- Lyubarsky, Y. E. 2002, *MNRAS*, 332, 199
- Lyutkov, M. 2006, *MNRAS*, 367, 1594
- McGarry, M. B., Gaensler, B. M., Ransom, S. M., Kaspi, V. M., & Veljkovic, S., *ApJ*, 627, L137
- McLaughlin, M. A., et al. 2003, *ApJ*, 591, L135
- Majid, W. A., Lamb, R. C., & Macomb, D. J. 2004, *ApJ*, 609, 133
- Markwardt, C., et al. 2005, *GRB Coord. Netw. Circ.*, 4037
- Marsden, D., & White, N. E. 2001, *ApJ*, 551, L155
- Mazets, E. P., Golenetskii, S. V., & Gur'yan, Yu. A. 1979, *Soviet Astron. Lett.*, 5, 343
- Mazets, E. P., Cline, T. L., Aptekar, R. L., Butterworth, P. S., Frederiks, D. D., Golenetskii, S. V., Il'inskii, V. N., & Pal'shin, V. D., *Astron. Lett.*, 25, 635
- Mazets, E. P., Cline, T. L., Aptekar, R. L., Frederiks, D. D., Golenetskii, S. V., Il'inskii, V. N., Pal'shin, V. D. 2005, arXiv: astro-ph/050254
- Mereghetti, S., Tiengo, A., Stella, L., Israel, G. L., Rea, N., Zane, S., & Oosterbroek, T. 2004, *ApJ*, 608, 42
- Mereghetti, S., et al. 2005, *ApJ*, 628, 938
- Mereghetti, S., et al. 2006a, *ApJ*, 653, 1423
- Mereghetti, S., et al. 2006b, *A&A*, 450, 759
- Mereghetti, S., Esposito, P., & Tiengo, A. 2007, *Ap&SS*, 308, 13

- Mereghetti, S., Paizis, A., Gotz, D., Petry, D., Shaw, S., Beck, M., & Borkowski J. 2007, GRB Coord. Netw. Circ., 6927
- Minter, A. H., Camilo, F., Ransom, S. M., Halpern, J. P., & Zimmerman, N. 2007, arXiv: astro-ph/0705.4403
- Mitsuda, K., et al. 2007, PASJ, 59, S1
- Molkov, S., Hurley, K., Sunyaev, R., Shtykovsky, P., Revnivtsev, M., & Kouveliotou, C. 2005, A&A, 433, L13
- Morii, M., Sato, R., Kataoka, J., & Kawai, N. 2003, PASJ, 55, L45
- Muno, M. P., et al. 2006, ApJ, 636, L41
- Muno, M. P., Gaensler, B. M., Clark, J. S., de Grijs, R., Pooley, D., Stevens, I. R., & Portegies Zwart, S. F. 2007, MNRAS, 378, L44
- Naik, S., et al. 2008, PASJ, 60, 237
- Nakagawa, Y. E., et al. 2007, PASJ, 59, 653
- Nakagawa, Y. E. 2007, Ph.D. Thesis, Aoyama Gakuin University
- Olive, J. -F., Hurley, K., Sakamoto, T., Atteia, J. -L., Crew, G., Ricker, G., Pizzichini, G., & Barraud, C. 2004, ApJ, 616, 1148
- Oosterbroek, T., Parmar, A. N., Rea, N., Israel, G. L., Stella, L., Mereghetti, S., Haberl, F., & Angelini, L. 2004, in The 5th INTEGRAL Workshop - The INTEGRAL Universe, ed. V.Schönfelder, G. Lichti & C. Winkler (Noordwijk: ESA Publication Division), 471
- Paczyński, B. 1992, Acta Astron., 42, 145
- Palmer, D. M., et al. 2005, Nature, 434, 1107
- Park, S., et al. 2006, ApJ, 653, L37
- Patel, S. K., et al. 2001, ApJ, 563, L45
- Patel, S. K., et al. 2003, ApJ, 587, 367
- Patel, S. K., et al. 2007, ApJ, 657, 994
- Perna, R., Heyl, J. S., Hernquist, L. E., Juett, A. M., & Chakrabarty, D. 2001, ApJ, 557, 18
- Pivovarov, M. J., & Kaspi, V. M. 2000, ApJ, 535, 379
- Rea, N., Israel, G. L., Steall, L., Oosterbroek, T., Mereghetti, S., Angelini, L., Campana, S., & Covino, S., ApJ, 586, L65
- Rea, N., et al. 2007, Ap&SS, 308, 505
- Romano, P., et al. 2006, A&A, 456, 917
- Seward, F. D., Charles, P. A., & Smale, A. P. 1986, ApJ, 305, 814
- Shimizu, T. 1995, PASJ, 47, 251
- Shirasaki, Y., et al. 2003, PASJ, 55, 1033
- Snowden, S. L. 2002, arXiv: astro-ph/0203311
- Snowden, S., Immler, S., Arida, M., Perry, B., Still, M., & Harrus, I. 2004, THE XMM-NEWTON ABC GUIDE, Version 2.01, 21
- Sonobe, T., Murakami, T., Kulkarni, S. R., Aoki, T., & Yoshida, A. 1994, ApJ, 436, L23
- Sugizaki, M., Nagase, F., Torii, K., Kinugawa, K., Asanuma, T., Matsuzaki, K., Koyama, K., & Yamauchi, S. 1997, PASJ, 49, L25
- Sugizaki, M., Mitsuda, K., Kaneda, H., Matsuzaki, K., Yamauchi, S., & Koyama, K. 2001, ApJ, 134, 77
- Strüder, L., et al. 2001, A&A, 365, L18
- Takahashi, T., et al. 2007, PASJ, 59, S35
- Tam, C. R., Kaspi, V. M., Gaensler, B. M., & Gotthelf, E. V. 2006, ApJ, 652, 548
- Tanaka, Y. T., Terasawa, T., Kawai, N., Yoshida, A., Yoshikawa, I., Saito, Y., Takashima, T., & Mukai, T. 2007, arXiv: astro-ph/0706.3123
- Terasawa, T., et al. 2005, Nature, 434, 1110
- Thompson, C., & Duncan, R. 1995, MNRAS, 275, 255
- Thompson, C., & Duncan, R. 1996, ApJ, 473, 322
- Thompson, C., & Duncan, R. 2001, ApJ, 561, 980
- Tian, W. W., & Leahy, D. A. 2008, ApJ, 677, 292
- Tiengo, A., Göhler, E., Staubert, R., & Mereghetti, S. 2002, A&A, 383, 182
- Tiengo, A., Mereghetti, S., Turolla, R., Zane, S., Rea, N., Stella, L., Israel, L. 2005, A&A, 437, 997
- Tiengo, A., Mereghetti, S., Esposito, P., De Luca, A., Gotz, D. 2007, The Astronomer's Telegram, 1243
- Turner, M. J. L., et al. 2001, A&A, 365, L27
- Vasisht, G., & Gotthelf, E. V. 1997, ApJ, 486, L129
- Wachter et al. 2004, ApJ, 615, 887
- Woods, P., et al. 2004, ApJ, 605, 378
- Woods, P. M., & Thompson, C. 2006, in Compact Stellar X-Ray Sources, ed. W. H. Lewin & M. van der Klis (Cambridge: Cambridge University Press), ch. 14
- Yamazaki, R., Ioka, K., Takahara, F., & Shibasaki, N., PASJ, 57, L11
- Yuda, S., Hiei, E., Takahashi, M., & Watanabe, T. 1997, PASJ, 49, 115